AMERICAN JOURNAL OF BIOSCIENCE AND CLINICAL INTEGRITY
https://biojournals.us/index.php/AJBCI
ISSN: 2997-7347

Article

Tetrazoles and Pyrimidines: Preparation Methods, Spectroscopic Characterization, and Biological Importance

Mutlaq Saud Khalaf [1]
[1] Ministry of Education, General Directorate of Education of Salah al-Din, Iraq
*Correspondence: mtlkswdalljy@gmail.com

Citation: Khalaf, M. S. Tetrazoles and Pyrimidines: Preparation Methods, Spectroscopic Characterization, and Biological Importance. American Journal Of Bioscience And Clinical Integrity 2026, 3(7), 51-64

Received: 19th Apr 2026
Revised: 21st May 2026
Accepted: 08th June 2026
Published: 20th July 2026

Abstract: Tetrazoles and pyrimidines are nitrogen-rich heterocycles with broad importance in synthetic and medicinal chemistry. This study presents the preparation and spectroscopic characterization of representative tetrazole and pyrimidine derivatives and places the obtained compounds within the wider context of biologically active heterocycles. Pyrimidine derivatives (AD8–AD12) were synthesized by cyclocondensation of substituted chalcones with cyanoguanidine in ethanol in the presence of glacial acetic acid, whereas tetrazole derivatives were prepared through azide–nitrile or azide-assisted cyclization under heating. The products were isolated by precipitation, filtration, washing, and recrystallization. Their physical properties were evaluated from color, melting point, molecular formula, and isolated yield, while structural assignments were supported by Fourier-transform infrared spectroscopy and, for selected compounds, by ^{1}H and ^{13}C nuclear magnetic resonance data. The pyrimidine series gave isolated yields of 44–65%, and the tetrazole series gave yields of 55–70%. Diagnostic FTIR bands included N–H, aromatic C–H, C=N/C=C, N=N, C–N, and N–N vibrations, together with substituent-specific absorptions. The results support successful heterocycle formation and illustrate the value of both ring systems as adaptable scaffolds for further pharmacological evaluation. No direct antimicrobial assay was reported; therefore, biological relevance is discussed on the basis of established literature rather than inferred from the present synthetic data.

Keywords: tetrazole; pyrimidine; heterocyclic synthesis; FTIR spectroscopy; medicinal chemistry.

Introduction

Tetrazoles are five-membered aromatic heterocycles composed of one carbon atom and four nitrogen atoms. Their high nitrogen content, tautomerism, acidity, and capacity for multiple hydrogen-bonding interactions make them valuable in synthetic chemistry, coordination chemistry, and drug design. In medicinal chemistry, 5-substituted tetrazoles are widely employed as metabolically stable bioisosteres of carboxylic acids.

Figure 1. Structural relationship among the diazine isomers pyrimidine, pyrazine, and pyridazine.

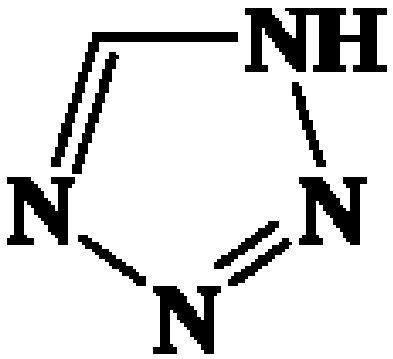

Figure 2. Parent tetrazole ring system.

A common and practical route to 5-substituted tetrazoles is the [3+2] cycloaddition of azide to a nitrile. Safer variants employ sodium azide with a suitable catalyst or promoter, and the broad substrate scope of the nitrile–azide transformation has been demonstrated for aromatic and aliphatic nitriles. Representative transformations are summarized in Figures 3–6.

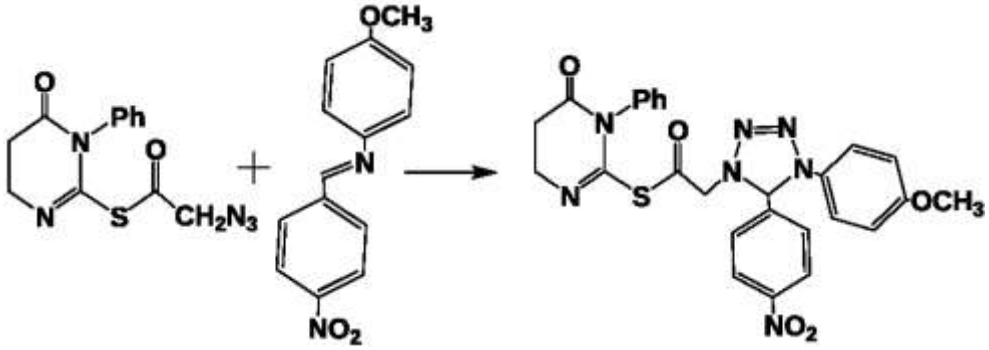

Figure 3. Cycloaddition route to a substituted tetrazole derivative.

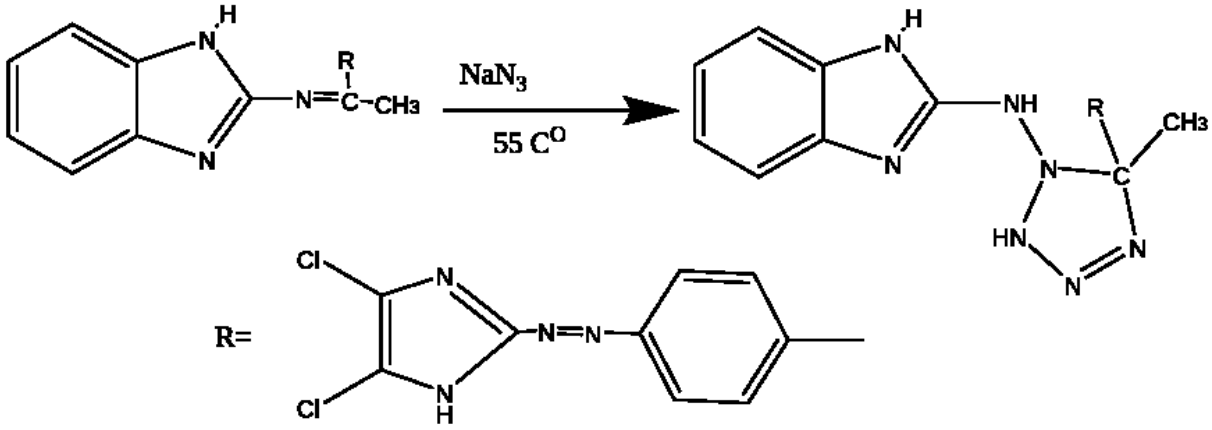

Figure 4. Tetrazole formation from a Schiff-base precursor and sodium azide.

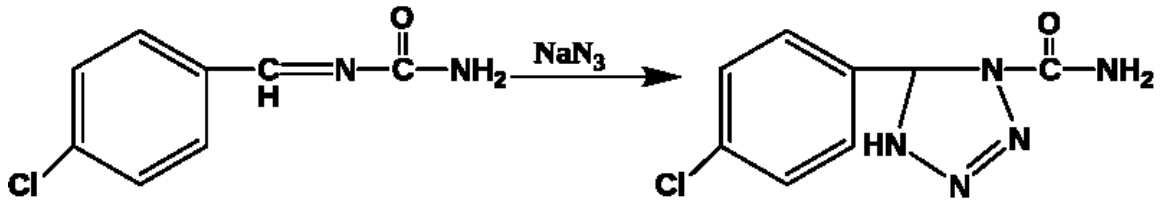

Figure 5. Sodium-azide cyclization of an acyl-hydrazone derivative.

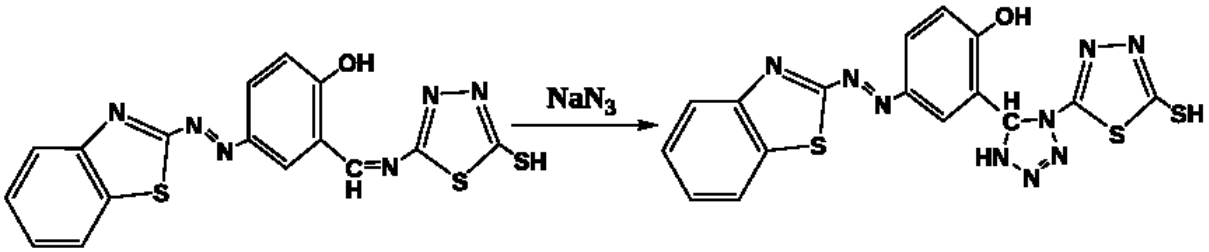

Figure 6. Tandem azide addition and cyclization leading to a fused tetrazole derivative.

Pyrimidine is a six-membered 1,3-diazine ring and is a fundamental structural unit in cytosine, thymine, uracil, nucleosides, nucleotides, and numerous natural products. The electron-deficient aromatic ring is readily functionalized, and diverse pyrimidine derivatives can be prepared through condensation or cyclization reactions involving amidines, guanidines, ureas, thioureas, nitriles, and carbonyl compounds.

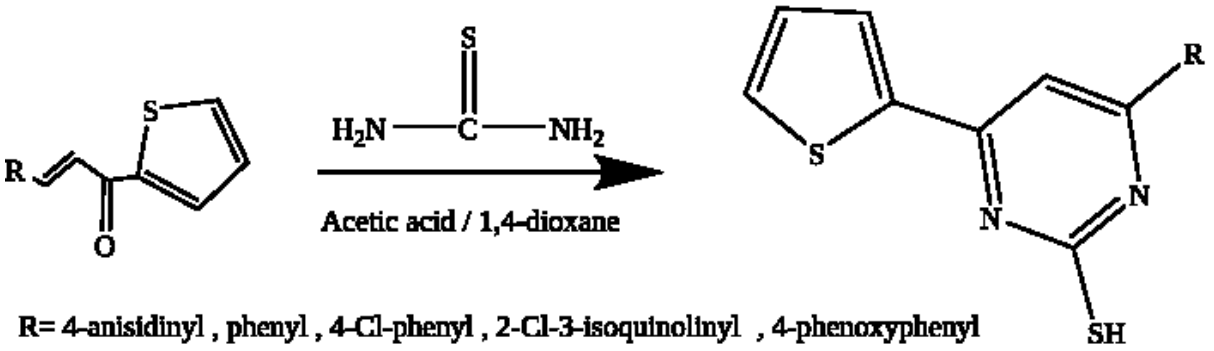

Figure 7. Thiopyrimidine synthesis from a chalcone-type precursor and thiourea.

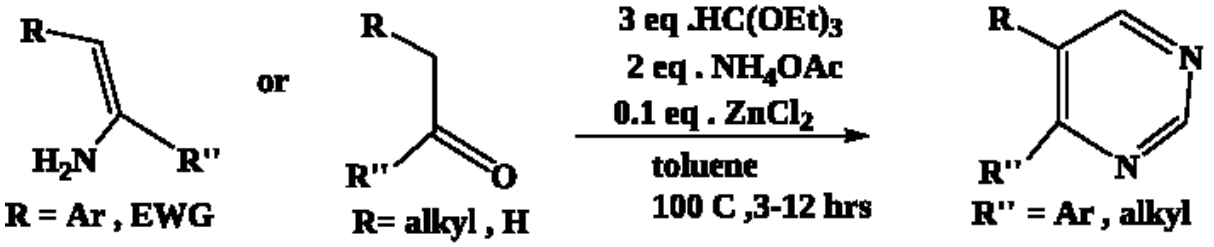

Figure 8. $ZnCl_2$-catalyzed pyrimidine formation from enamine or ketone precursors.

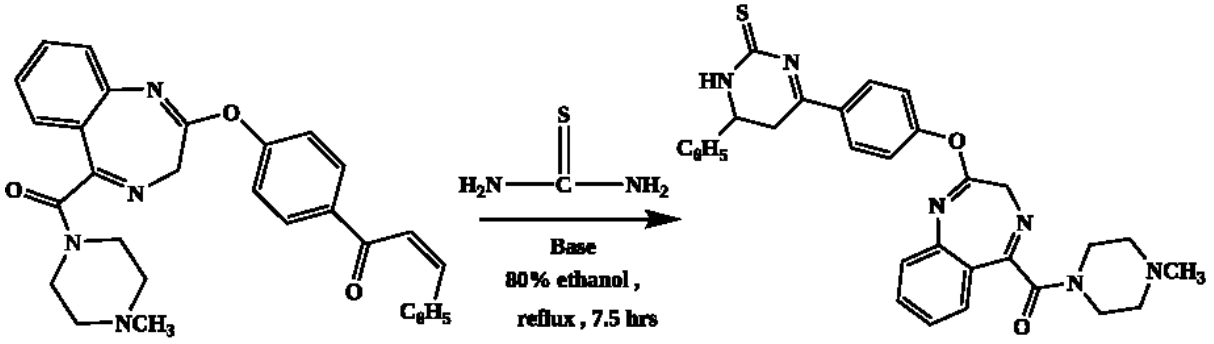

Figure 9. Thiourea-mediated synthesis of a fused thiopyrimidine derivative.

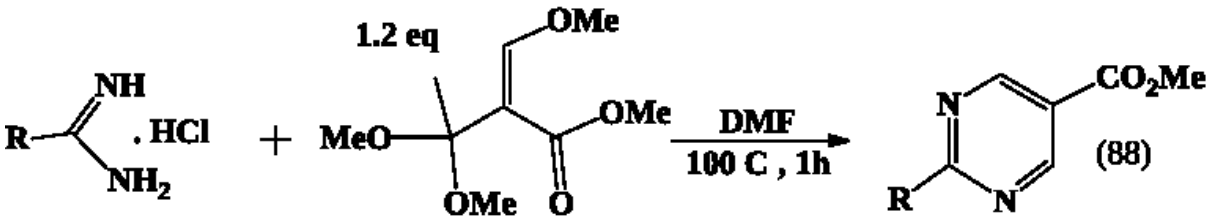

Figure 10. Formation of pyrimidine-5-carboxylate esters from amidinium salts.

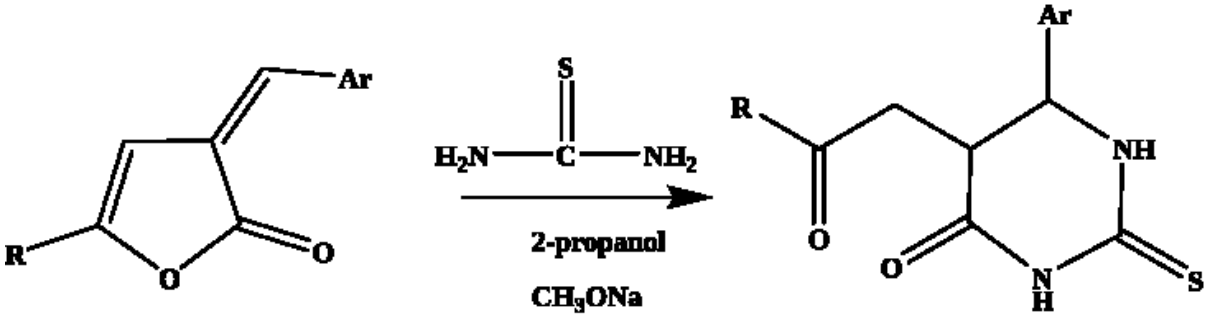

R= 4-Tol , Ar = 3-$NO_2C_6H_4$, 2-ClC_6H_4

R= 4-$CH_3OC_6H_4$, Ar = 3-$NO_2C_6H_4$, 2-ClC_6H_4 , 4-$CH_3OC_6H_4$

Figure 11. Synthesis of substituted thiopyrimidinediones from enone precursors and thiourea.

Both ring systems occur in biologically important molecules. Tetrazole-containing compounds have been explored as antihypertensive, antimicrobial, anti-inflammatory, and anticancer agents, while pyrimidine derivatives are represented among anti-infective, anticancer, antiviral, anti-inflammatory, analgesic, neurological, and metabolic therapeutics. The representative scaffolds in Figures 12–15 illustrate the structural diversity associated with these applications; however, the biological activity of the compounds synthesized in the present study was not experimentally assessed.

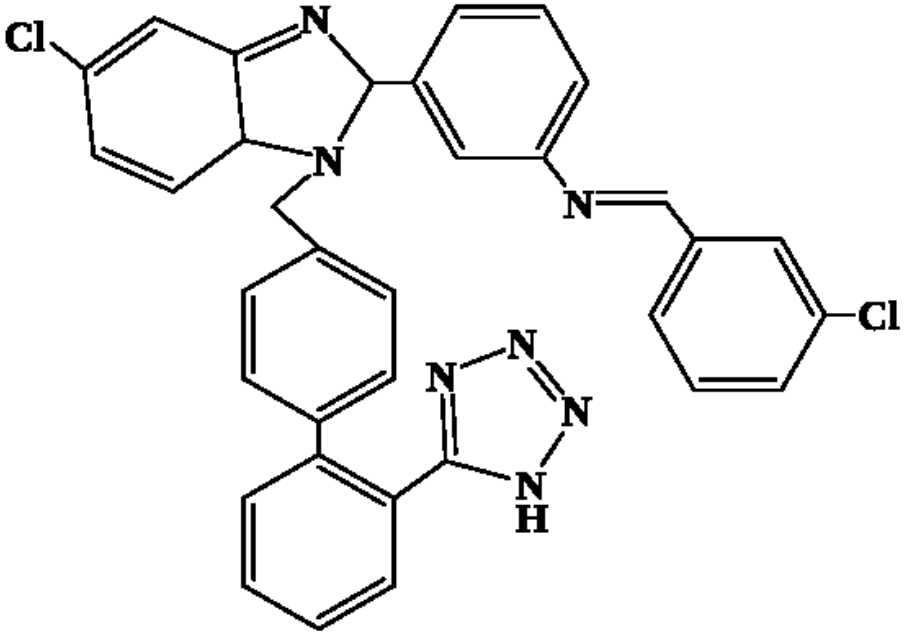

Figure 12. Representative tetrazole-containing bioactive scaffold.

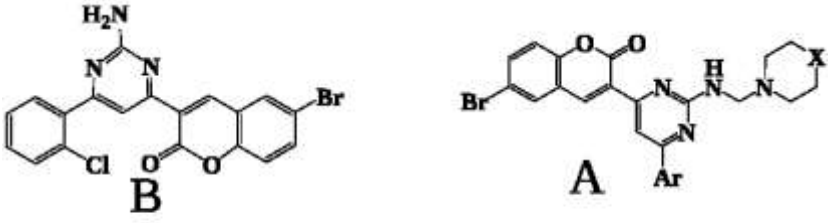

Figure 13. Representative pyrimidine derivatives A and B associated with reported biological activity.

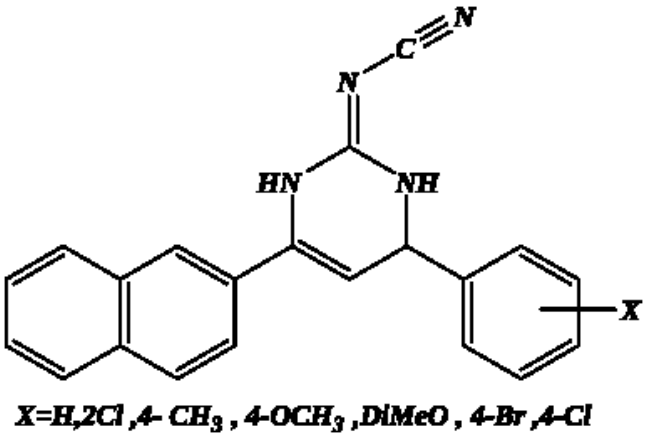

C

Figure 14. Representative pyrimidine derivative C.

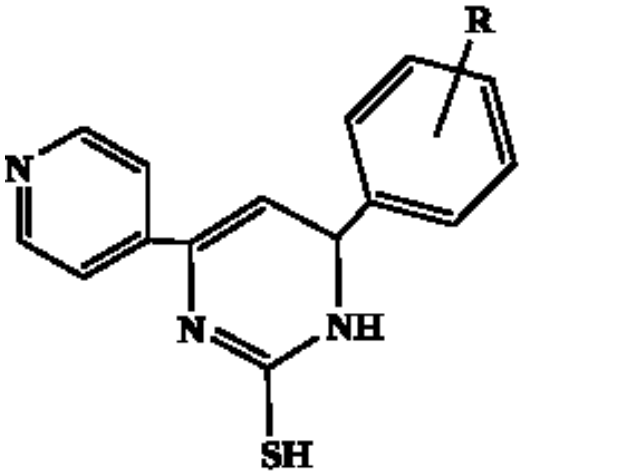

D

Figure 15. Representative thiopyrimidine derivative D.

Interdisciplinary Context of the Supplied References

The supplied bibliography includes studies of tumor–immune interactions, tumor immunology, programmed cell death, immune escape, and tumor-microenvironment diversity [1], [3], [9], [12], [14], [23], [24]. These sources provide a broad biological context for understanding complex

disease processes, but they do not directly establish the synthesis or spectroscopic characterization of tetrazole and pyrimidine derivatives.

It also contains foundational and generalized work on species interaction, mass-action dynamics, chemotaxis, ecological systems, random competitive environments, mathematical-biology theory, and the control or numerical solution of predator–prey and epidemic models [2], [4], [5], [6], [7], [8], [10], [11], [13], [15], [16], [17], [18], [19], [20], [21], [22]. These mathematical frameworks may support future pharmacodynamic or systems-level investigations after biological data are available.

More recent contributions examine modified, stochastic, reaction–diffusion, and disease-coupled predator–prey systems, together with transform-based and stability-analysis techniques [25], [26], [27], [28], [29]. Additional studies address partial differential equations, thin-film and micropolar-fluid models, acceleration methods for integral equations, and finite-difference schemes [30], [31], [32], [33], [34]. They are therefore cited only as interdisciplinary methodological context and should not be interpreted as direct chemical evidence for the compounds reported in this study.

The objective of this study was to synthesize representative tetrazole and pyrimidine derivatives, document their physical properties, and evaluate their structural features using FTIR and selected NMR data.

Materials and Methods

Study Design and Materials

The work was designed as a laboratory-scale synthetic and characterization study. Reagents included substituted chalcones, cyanoguanidine, ethanol, glacial acetic acid, benzonitrile, sodium azide, ammonium chloride as a weak-acid promoter, dilute hydrochloric acid, water, crushed ice, dioxane, and triethylamine. The original laboratory record did not provide manufacturers, grades, or instrument models; these details should be supplied by the author before final journal submission. Sodium azide reactions were conducted in a fume hood with appropriate personal protective equipment, and contact with heavy metals and strong acid under warm conditions was avoided because hazardous azide species may form.

Synthesis of Pyrimidine Derivatives AD8–AD12

Cyanoguanidine (0.04 g) was dissolved in ethanol (10 mL), and several drops of glacial acetic acid were added. The mixture was stirred for 15 min. A substituted chalcone (AD3–AD7, 0.002 mol) was then introduced, and the reaction mixture was heated under reflux for 2.5 h. The volume was reduced to approximately one-third, the mixture was cooled, and the concentrate was poured onto crushed ice. After standing for 8 h, the precipitated product was collected by filtration, washed, and recrystallized from ethanol. The isolated compounds were labeled AD8–AD12.

Synthesis of Tetrazole Derivatives

Benzonitrile (1.0 g) was combined with sodium azide (0.72–0.98 g), added portionwise to ensure controlled reaction and complete consumption of the nitrile. Ammonium chloride (0.8 g) was used as a weak-acid promoter. The mixture was heated at 100–120 °C for 6–24 h with agitation, and reaction progress was monitored by thin-layer chromatography. After cooling to room temperature, the mixture was added to water and ice. Dilute hydrochloric acid was added cautiously to adjust the pH and liberate the free tetrazole. The precipitate was filtered, washed with cold water, and dried. Related tetrazoles AD53–AD58 were obtained by azide-assisted cyclization of hydrazone precursors in dioxane with triethylamine, as represented in Figure 16.

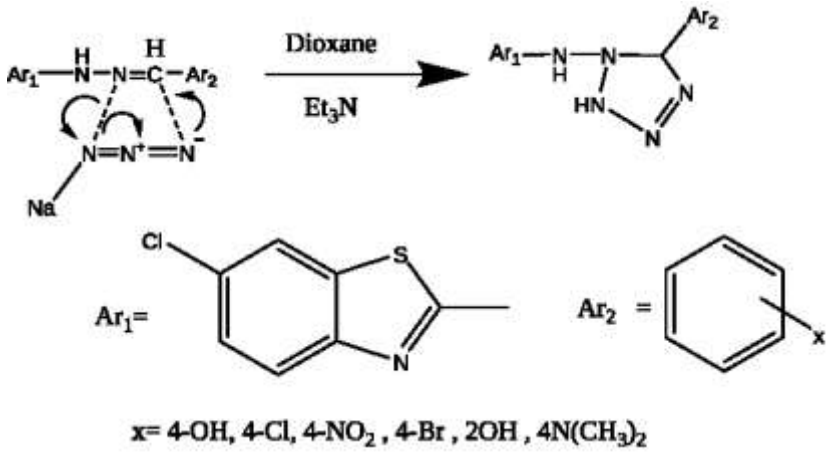

Figure 16. Proposed formation of tetrazole derivatives AD53–AD58 from hydrazone precursors.

Characterization and Data Treatment

Products were evaluated by appearance, melting-point range, molecular formula, and isolated yield. FTIR spectra were recorded using KBr preparations over the mid-infrared region, and the principal bands were assigned to N–H, O–H, aromatic C–H, aliphatic C–H, C=C, C=N, N=N, C–N, N–N, and substituent-specific vibrations. Selected compounds were additionally assessed by ^{1}H and ^{13}C NMR spectroscopy in DMSO-d_6. Data analysis was descriptive; no inferential statistical test was applied because the study did not include replicated biological assays or treatment groups.

Results

Physical Properties and Yields

The pyrimidine derivatives AD8–AD12 were isolated as brown to orange solids with melting points ranging from 174 to 262 °C and yields of 44–65% (Table 1). The tetrazole derivatives TZ-1–TZ-5 were obtained as white to light-yellow solids, with melting points of 140–198 °C and yields of 55–70% (Table 2).

Table 1. Physical properties and isolated yields of pyrimidine derivatives AD8–AD12.

Compound	Substituent (X)	m.p. (°C)	Yield (%)	Color	Molecular formula
AD8	4-OH	198–200	65	Brown	$C_{24}H_{16}ClFN_7O_2S$
AD9	3,4-$(OCH_3)_2$	223–225	50	Brown	$C_{26}H_{21}ClN_7O_3S$
AD10	2,4-$(OH)_2$	260–262	44	Brown	$C_{24}H_{16}ClN_7O_3S$
AD11	4-NO_2	174–176	54	Orange	$C_{24}H_{15}ClN_7O_3S$
AD12	4-F	190–192	60	Brown	$C_{24}H_{15}ClFN_7OS$

Table 2. Physical properties and isolated yields of tetrazole derivatives TZ-1–TZ-5.

Compound	Substituent (X)	m.p. (°C)	Yield (%)	Color	Molecular formula
TZ-1	H	150–152	70	White	CH_2N_4
TZ-2	CH_3	165–167	65	Light yellow	$C_2H_4N_4$
TZ-3	Cl	180–182	60	White	$CHClN_4$

Compound	Substituent (X)	m.p. (°C)	Yield (%)	Color	Molecular formula
TZ-4	NO_2	195–198	55	Yellow	$CH_2N_6O_2$
TZ-5	OCH_3	140–143	62	White	$C_2H_4N_4O$

Spectroscopic Characterization of Tetrazoles AD53–AD58

The FTIR spectra of AD53–AD58 showed aromatic C–H absorptions at 3060–3095 cm^{-1}, C=C bands at 1598–1614 cm^{-1}, N=N bands at 1436–1517 cm^{-1}, C–N bands at 1342–1396 cm^{-1}, and N–N bands at 1093–1121 cm^{-1}. Substituent-specific absorptions included O–H, C–Cl, NO_2, C–Br, and aliphatic C–H bands (Table 3).

Table 3. FTIR absorption bands of tetrazole derivatives AD53–AD58 (cm^{-1}, KBr).

Comp.	Aryl group	N–H	Ar–H	C=C	N=N	C–N	N–N	Other
AD53	4-OH-C_6H_4	3400	3060	1612	1436	1349	1112	3450 (O–H)
AD54	4-Cl-C_6H_4	3390	3090	1601	1490	1359	1121	813 (C–Cl)
AD55	4-NO_2-C_6H_4	3440	3070	1598	1517	1342	1101	1255 (NO_2)
AD56	4-Br-C_6H_4	3399	3095	1600	1510	1350	1112	671 (C–Br)
AD57	2-OH-C_6H_4	3398	3076	1614	1463	1396	1093	3230 (O–H)
AD58	4-$N(CH_3)_2$-C_6H_4	3413	3074	1604	1438	1359	1093	2947–2833 (aliphatic C–H)

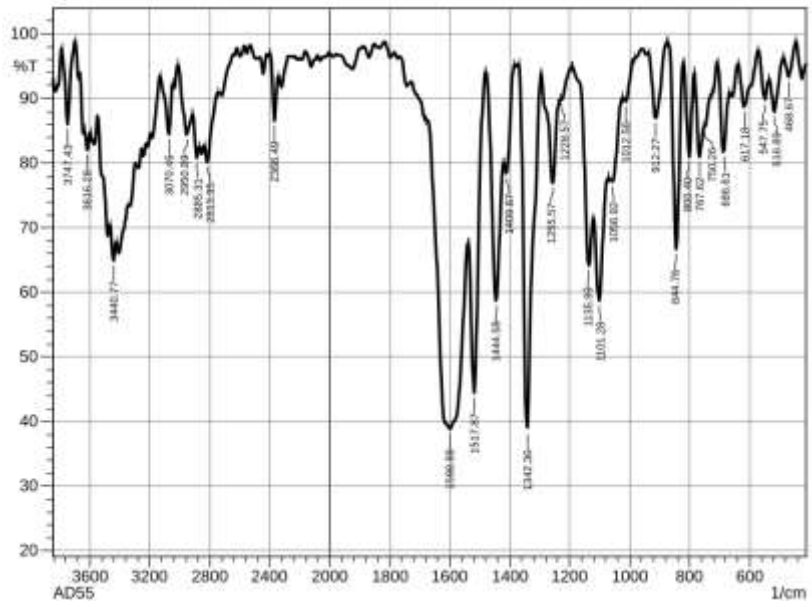

Figure 17. FTIR spectrum of tetrazole derivative AD55.

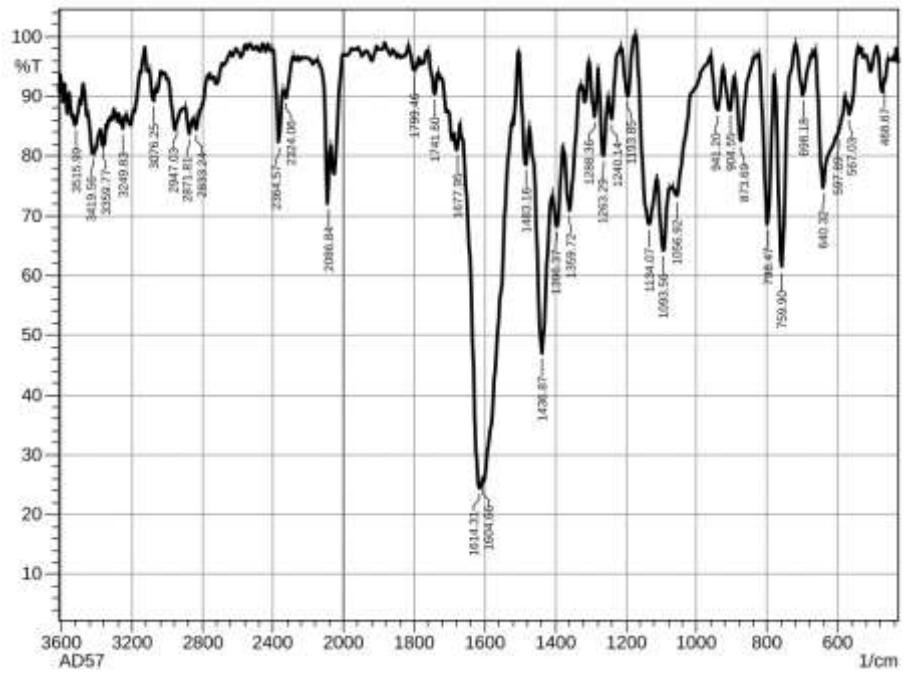

Figure 18. FTIR spectrum of tetrazole derivative AD57.

For compound AD53, the ^{1}H NMR spectrum contained a signal at δ 3.80 ppm assigned to N–H and multiplets at δ 6.83–8.38 ppm assigned to aromatic protons. The ^{13}C NMR spectrum contained a signal at δ 167.99 ppm attributed to the tetrazole-ring carbon and signals at δ 116.26–131.83 ppm for aromatic carbons. A residual DMSO signal appeared near δ 2.50 ppm.

Spectroscopic Characterization of Pyrimidines AD8–AD12

The pyrimidine products were formed by cyclocondensation of chalcones with cyanoguanidine, as summarized in Figure 19. The proposed sequence involves conjugate addition, tautomerization, ring closure, and dehydration (Figure 20).

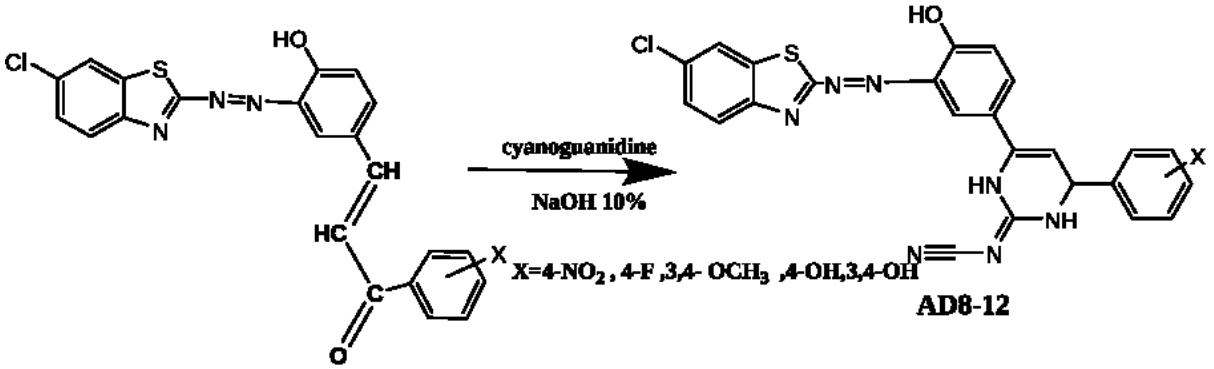

Figure 19. General synthesis of pyrimidine derivatives AD8–AD12 from chalcone precursors and cyanoguanidine.

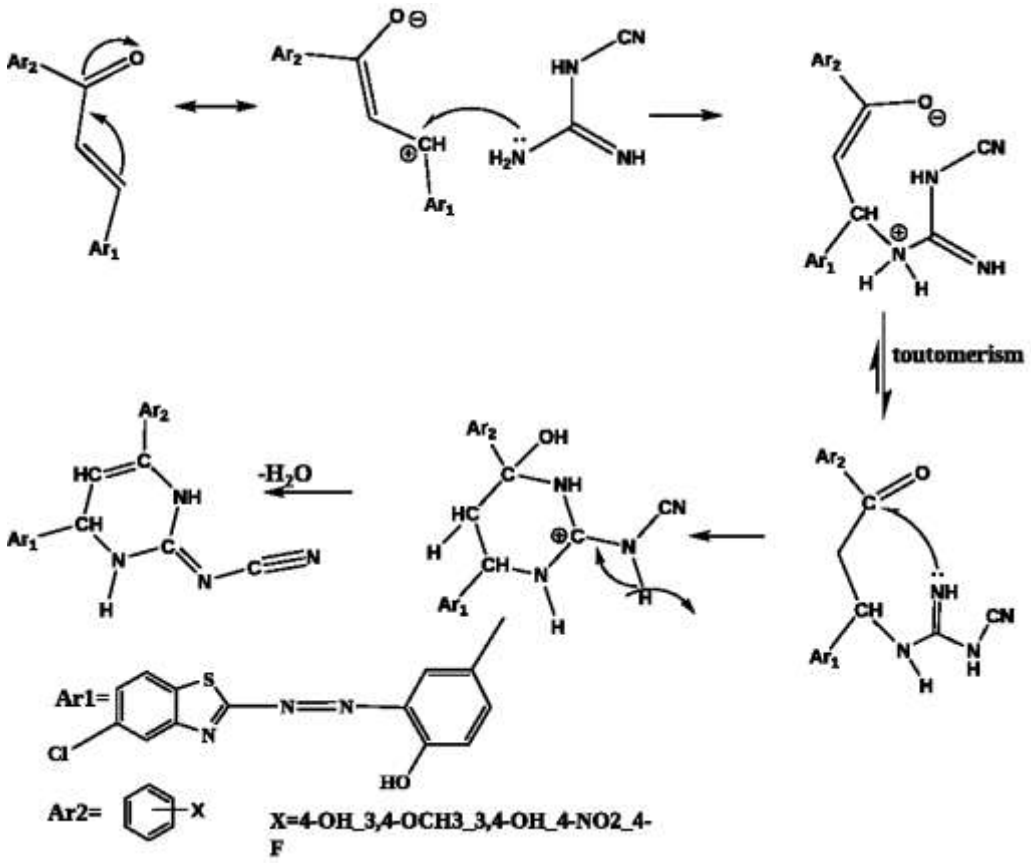

Figure 20. Proposed mechanism for pyrimidine-ring formation.

The FTIR spectra of AD8–AD12 displayed N–H absorptions at 3251–3370 cm^{-1}, aromatic C–H bands at 2923–3087 cm^{-1}, C=N bands at 1589–1643 cm^{-1}, and C=C bands at 1521–1533 cm^{-1} (Table 4). Substituent-specific bands supported the presence of hydroxy, nitro, and fluoro groups.

Table 4. FTIR absorption bands of pyrimidine derivatives AD8–AD12 (cm^{-1}, KBr).

Compound	X	N–H	Ar–H	C=N	C=C	Other
AD8	4-OH	3272	3087	1633	1533	3456 (O–H, broad)
AD9	3,4-$(OCH_3)_2$	3271	3083	1633	1533	—
AD10	2,4-$(OH)_2$	3370	2923	1643	1529	3300 (O–H, broad)
AD11	4-NO_2	3294	3074	1589	1521	1344 (NO_2, symmetric)
AD12	4-F	3251	3062	1612	1523	790 (C–F)

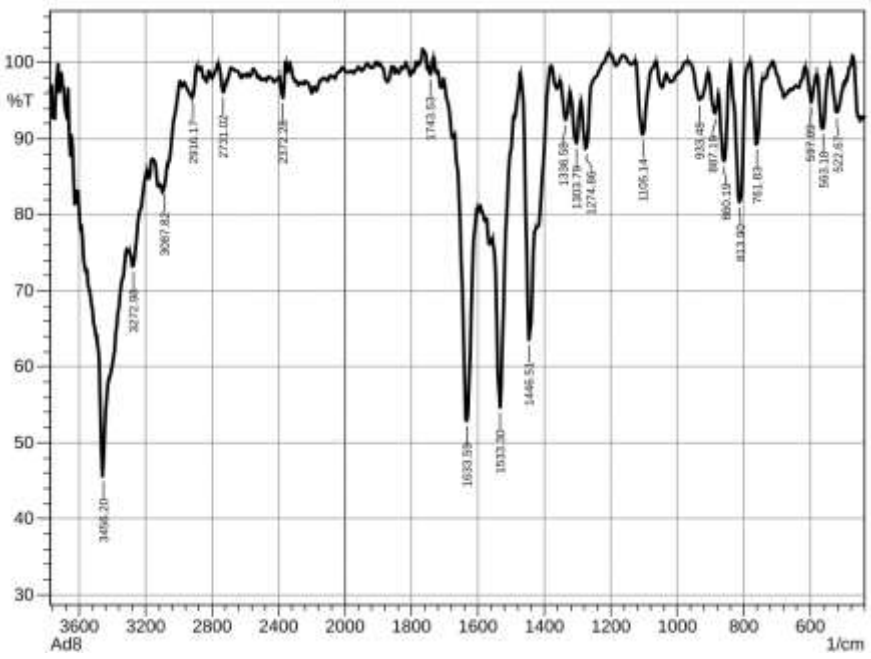

Figure 21. FTIR spectrum of pyrimidine derivative AD8.

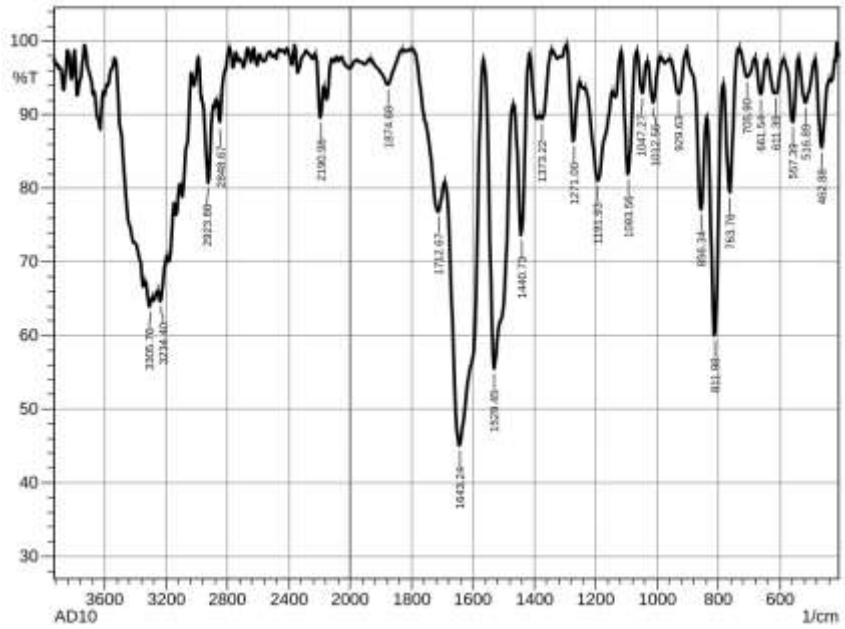

Figure 22. FTIR spectrum of pyrimidine derivative AD10.

For compound AD10, the ^{1}H NMR spectrum showed a signal near δ 5.84 ppm assigned to N–H, a signal at δ 8.62 ppm assigned to the pyrimidine C–H proton, hydroxy and additional N–H signals near δ 9.11 and 9.79 ppm, and aromatic multiplets at δ 6.66–8.64 ppm. The ^{13}C NMR data included resonances at δ 29.46, 119.04, and 152.23 ppm assigned to pyrimidine-ring carbons, together with aromatic carbon signals at δ 124.96–126.01 ppm.

Discussion

The isolated yields indicate that both synthetic routes were operational under the reported conditions, although the tetrazole series generally gave slightly higher yields than the pyrimidine series. The 55–70% tetrazole yields are consistent with the broad utility of nitrile–azide cycloaddition methods, while the 44–65% pyrimidine yields reflect the multiple condensation, cyclization, and

dehydration steps involved in ring construction. Differences among substituents may arise from electronic effects, substrate solubility, precipitation efficiency, and product losses during recrystallization.

The tetrazole FTIR profiles provide complementary evidence for ring formation. Bands assigned to N=N, C–N, and N–N vibrations occurred consistently across AD53–AD58, while the ring-carbon resonance of AD53 at δ 167.99 ppm further supported a tetrazole environment. The combination of heterocycle-related bands with substituent-specific absorptions is more informative than any single peak and is consistent with the structural features expected for substituted tetrazoles.

For AD8–AD12, the appearance of N–H and C=N bands together with the retained aromatic features supports cyclization to a pyrimidine framework. The AD10 NMR data also indicate a heterocyclic C–H environment and multiple exchangeable protons. These findings agree with the established versatility of pyrimidine-forming condensations and the ease with which substitution patterns can be varied around the ring.

The medicinal relevance of the two scaffolds is well established but should be interpreted separately from the present analytical results. Tetrazoles are frequently used to replace carboxylic acids in drug candidates because they can retain acidity and target binding while modifying metabolic and physicochemical properties. Pyrimidines are present in nucleobases and in numerous approved or investigational drugs spanning anti-infective, anticancer, neurological, inflammatory, and metabolic indications. These precedents justify subsequent biological screening of the synthesized derivatives.

A major limitation is the absence of raw spectra, complete NMR assignments, elemental analysis, mass spectrometry, purity data, replicate yields, and direct antimicrobial or pharmacological assays. Consequently, the present study supports synthesis and preliminary structural characterization but does not establish biological efficacy. Future work should report instrument models and manufacturers, optimize reaction conditions, confirm structures using high-resolution mass spectrometry and complete 2D NMR, determine purity by chromatographic methods, and evaluate biological activity with appropriate positive controls, replicates, and statistical analysis.

Conclusion

Representative tetrazole and pyrimidine derivatives were synthesized and characterized using physical properties, FTIR spectroscopy, and selected NMR observations. The pyrimidine compounds AD8–AD12 were obtained in 44–65% yield, whereas tetrazole derivatives TZ-1–TZ-5 were obtained in 55–70% yield. Diagnostic FTIR absorptions and the available NMR signals were consistent with the proposed heterocyclic frameworks and substituents. The study demonstrates accessible routes to two biologically important classes of nitrogen heterocycles. Nevertheless, biological activity cannot be concluded from the current dataset because no direct bioassay was provided; such evaluation remains a priority for future research.

REFERENCES

[1] S. Kartal, “Mathematical modeling and analysis of tumor-immune system interaction by using Lotka-Volterra predator-prey like model with piecewise constant arguments,” Periodicals of Engineering and Natural Sciences, vol. 2, no. 1, 2014.

[2] V. Volterra, “Fluctuations in the abundance of a species considered mathematically,” Nature, vol. 118, pp. 558–560, 1926.

[3] R. P. Jiménez, L. E. Bergues Cabrales, and J. I. Montijano, “Dynamics of the Lotka-Volterra model for tumor-host systems under constant or periodic perturbation: Implications for cancer therapy,” Mar. 14, 2025.

[4] G. Craciun, F. Nazarov, and C. Pantea, “Persistence and permanence of mass-action and power-law dynamical systems,” SIAM Journal on Applied Mathematics, vol. 73, pp. 305–329, 2013.

[5] L. Xie and Y. Wang, “On a fully parabolic chemotaxis system with Lotka-Volterra competitive kinetics,” Journal of Mathematical Analysis and Applications, vol. 471, pp. 584–598, 2019.

[6] K. Su, C. Wang, S. Zhang, and S. Liu, "Lotka-Volterra equation-based modeling of the aerobic granulation process in sequencing batch reactors," International Biodeterioration & Biodegradation, vol. 115, pp. 49–54, 2016.
[7] R. A. Cropp and J. Norbury, "Population interactions in ecology: A rule-based approach to modeling ecosystems in a mass-conserving framework," SIAM Review, vol. 57, pp. 437–446, 2015.
[8] C. Li and H. Zhu, "Canard cycles for predator-prey systems with Holling types of functional response," Journal of Differential Equations, vol. 254, pp. 879–910, 2013.
[9] B. M. Holzapfel, F. Wagner, L. Thibaudeau, J.-P. Levesque, and D. W. Hutmacher, "Concise review: Humanized models of tumor immunology in the 21st century: Convergence of cancer research and tissue engineering," Stem Cells, vol. 33, no. 6, pp. 1696–1704, 2015.
[10] C. Zhu and G. Yin, "On competitive Lotka-Volterra model in random environments," Journal of Mathematical Analysis and Applications, vol. 357, pp. 154–170, 2009.
[11] V. Badri, M. J. Yazdanpanah, and M. S. Tavazoei, "Global stabilization of Lotka-Volterra systems with interval uncertainty," IEEE Transactions on Automatic Control, vol. 64, pp. 1209–1213, 2018.
[12] A. Wang, D. Xue, Z. Wang, J. Zhao, and F. Rao, "Dynamics of a stochastic tumor-immune interaction system," The European Physical Journal Plus, vol. 139, 2024.
[13] J. D. Murray, Mathematical Biology I: An Introduction, 3rd ed. New York, NY, USA: Springer, 2002.
[14] J. Liu, M. Hong, Y. Li, D. Chen, Y. Wu, and Y. Hu, "Programmed cell death tunes tumor immunity," Frontiers in Immunology, vol. 13, 2022.
[15] J. Biazar and R. Montazeri, "A computational method for solution of the prey and predator problem," Applied Mathematics and Computation, vol. 163, no. 2, pp. 841–847, 2005.
[16] L. Bougoffa, "Solvability of the predator and prey system with variable coefficients and comparison of the results with modified decomposition," Applied Mathematics and Computation, vol. 182, no. 1, pp. 383–387, 2006.
[17] M. S. H. Chowdhury, I. Hashim, and S. Mawa, "Solution of the predator-prey problem by a numerical-analytic technique," Communications in Nonlinear Science and Numerical Simulation, vol. 14, no. 4, pp. 1008–1012, 2009.
[18] O. D. Makinde, "Solving a ratio-dependent predator-prey system with constant-effort harvesting using the Adomian decomposition method," Applied Mathematics and Computation, vol. 186, no. 1, pp. 17–22, 2007.
[19] E. Yusufoglu and E. Baris, "He's variational iteration method applied to the solution of the prey and predator problem with variable coefficients," Physics Letters A, vol. 372, no. 21, pp. 3829–3835, 2008.
[20] V. S. Erturk and S. Momani, "Solutions to the predator-prey problem and the epidemic model via the differential transform method," Kybernetes, vol. 37, no. 8, pp. 1180–1188, 2008.
[21] A. R. Ghotbi, A. Barari, and D. D. Ganji, "Solving a ratio-dependent predator-prey system with constant-effort harvesting using the homotopy perturbation method," Mathematical Problems in Engineering, vol. 2008, pp. 1–7, 2008.
[22] T. Vijayalakshmi and S. Rathinam, "Application of homotopy perturbation and variational iteration methods for a nonlinear imprecise prey-predator model with stability analysis," The Journal of Supercomputing, vol. 78, no. 2, pp. 2477–2502, 2022.
[23] I. Poschke, D. Mougiakakos, and R. Kiessling, "Camouflage and sabotage: Tumor escape from the immune system," Cancer Immunology, Immunotherapy, vol. 60, no. 9, pp. 1221–1229, 2011.
[24] A. Bozyk, K. Wojas-Krawczyk, P. Krawczyk, and J. Milanowski, "Tumor microenvironment—A short review of cellular and interaction diversity," Biology, vol. 11, no. 6, p. 929, 2022.
[25] S. Jawad, D. Sultan, and M. Winter, "The dynamics of a modified Holling-Tanner prey-predator model with wind effect," International Journal of Nonlinear Analysis and Applications, vol. 12, Special Issue, pp. 2203–2210, 2021.
[26] M. W. Yasin, N. Ahmed, M. S. Iqbal, A. Raza, M. Rafiq, E. M. T. Eldin, and I. Khan, "Spatiotemporal numerical modeling of a stochastic predator-prey model," Scientific Reports, vol. 13, no. 1, p. 1990, 2023.
[27] Y. Sun and S. Chen, "Stability and bifurcation in a reaction-diffusion-advection predator-prey model," Calculus of Variations and Partial Differential Equations, vol. 62, no. 2, p. 61, 2023.

[28] M. S. Arif, K. Abodayeh, M. Shoaib, and A. Ejaz, "On the stability of the diffusive and nondiffusive predator-prey system with consuming resources and disease in prey species," Mathematical Biosciences and Engineering, vol. 20, no. 3, pp. 5066–5093, 2023.
[29] R. O. Al-Sadi and A. J. Al-Saif, "A new technique to solve predator-prey models using the Shehu transformation-Akbari-Ganji method with Padé approximants," Central Asian Journal of Mathematical Theory and Computer Sciences, vol. 4, no. 8, 2023.
[30] A. Ahadi, S. M. Mousavi, A. M. Alinia, and H. Khademi, Partial Differential Equations in Applied Mathematics, 2025.
[31] M. H. Hassan and A. J. Al-Saif, "A mathematical model for the velocity of thin film flow of a third-grade fluid down an inclined plane," Journal of Advanced Research in Fluid Mechanics and Thermal Sciences, vol. 102, no. 1, 2023.
[32] H. Mirgolbabae, S. T. Ledari, and D. D. Ganji, "Semi-analytical investigation on micropolar fluid flow and heat transfer in a permeable channel using AGM," Journal of the Association of Arab Universities for Basic and Applied Sciences, vol. 24, pp. 213–222, 2017.
[33] H. Mesgarani, N. Aghazadeh, and P. Parmour, "Aitken extrapolation and epsilon algorithm for an accelerated solution of weakly singular nonlinear Volterra integral equations," Physica Scripta, vol. 81, no. 1, p. 015001, 2010.
[34] A. Shah, L. Yuan, and A. Khan, "Upwind compact finite difference scheme for time-accurate solution of the incompressible Navier–Stokes equations," Applied Mathematics and Computation, vol. 215, pp. 3201–3213, 2010.